用于焊缝检测的比色图像偏心算法

高向东， 陈章兰， 陈永平
(广东工业大学 机电工程学院，广州 510090)


高向东

摘 要：提出了基于焊接比色图像偏心的概念并给出计算公式。从比色图像信号强度与焊接区域发射率、光谱辐射强度等的关系、比色值与焊接温度场及比色系统波长的关系以及比色图像偏心计算公式出发，分析了比色图像比色值分布对称性，推导并建立了焊接比色图像偏心与焊接区温度的函数值、焊缝中心与电弧中心偏差间关系模型。研究了以比色图像偏心作为检测对象的优异特性，给出了模型在某一焊接工艺参数条件下的数值解，发现模型的输出与输入有很好的线性关系。仿真试验证明以比色图像偏心可以代替焊缝中心偏差，为进一步研究比色图像偏心算法的实际应用打下理论基础。

关键词：比色图像；偏心；焊缝偏差；模型
中图分类号：TG316.7　　文献标识码：A　　文章编号：0253－360X(2006)05－013－05

0 序 言

焊接视觉传感法是焊接智能机器人系统实现焊缝自动跟踪、路径规划的重要传感方法，其算法的研究和应用主要集中在对焊缝图像的直接处理上。由于直接获取较清晰的焊缝图像非常困难，图像处理需要经过去噪、边缘检测及特征提取等技术，耗时较长，影响焊缝跟踪的实时性和精度。因此，寻找提取焊缝中心的易于检测的量，进而推测到难以提取的焊缝中心位置，对焊缝跟踪算法的简化和理论研究具有重要意义。焊接比色测温的原理是用两个不同波长滤光片同时摄取两幅图像，逐点求两幅图像的灰度比值，获得焊接区各点的真实温度，在焊接视觉测温中得到广泛应用[1]。

以 TIG 焊为研究对象，将比色测量方法应用于焊缝跟踪系统，提出了焊接比色图像偏心的概念并作为焊缝跟踪器的检测量，通过分析焊接区焊缝、金属区域的热辐射特点，推导出焊接比色图像偏心与焊接区各点温度、焊缝中心与电弧中心偏差的关系模型，从理论上研究了以比色图像偏心推算焊缝中心与电弧中心的偏差的可行性，为进一步深入研究比色图像偏心在焊缝跟踪系统中的实际应用奠定了基础。

1 焊接比色图像偏心算法基本原理

当电弧中心对准焊缝中心时，电弧热源的热流在两焊接上对称分布，焊接温度场关于电弧中心两侧对称；当电弧中心偏离焊缝中心时，这种对称关系被打破，电弧热源的热流在两焊件分布不再对称[2]，焊件上对称位置的热流密度会产生差异，从而关于电弧中心对称点处的温度值不再相等。视觉传感器所摄取到的灰度值及经计算后得到的图像比色值相应变化，焊接视觉跟踪算法的任务就是要探求焊缝中心位置的改变使温度场改变从而引起比色图像变化的对应关系。

设工件平面是 $x-y$（行 — 列）方向，视觉系统将熔池实时图像传入计算机并计算出焊缝中心，得到电弧中心与焊缝中心的偏差，计算机控制焊炬运动实现动态纠偏。

在 $x-y$ 平面内，焊接速度由 v_x、v_y 两个方面的焊接速度分量合成，当固定 y 方向焊接速度时，电弧与焊缝中心的偏差由 x 方向上偏差决定，因此只需计算 x 方向的偏差。

定义比色图像行 i 方向的偏心是以电弧中心为对称中心，求比色图像两侧比色值和位置的加权和与电弧中心线两侧比色值差值总和之商。比色图像偏心公式的离散表达式为

$$i_e=\frac{\sum_{j=1}^{n}\sum_{i=1}^{m}r(i,j)\cdot(i-i_c)}{\sum_{j=1}^{n}\sum_{i=1}^{m/2}r(i,j)-\sum_{j=1}^{n}\sum_{i=(m/2+1)}^{m}r(i,j)},\qquad(1)$$

式中：i_e 为焊接比色图像偏心值；i、j 分别为行和列；$r(i,j)$ 为比色图像 (i,j) 处比色值；m、n 分别为一行和一列中像素的数量；i_c 为电弧中心。

定义偏差为焊缝中心与电弧中心之差，式(1)表

收稿日期：2005－02－21
基金项目：国家自然科学基金资助项目(60375012)；广东省自然科学基金资助项目(020176)

明,当有偏差存在时,图像比色值分布的不对称程度通过偏心值表现出来。且对比色图像来说,获得某一时刻比色图像的比色值技术非常成熟,偏心值计算简单易得。

2 比色图像偏心与焊缝偏差的简化模型

当目标具有温度 T 时物体辐射源,通过中心波长 λ、带宽 $\Delta\lambda$ 的滤光片,在距离 R 处的光敏面上的信号强度 $Q(i,j)$[1] 为

$$Q(i,j)=\frac{u\varepsilon(i,j)C_1\Delta\lambda}{\lambda^5R^2}\{\exp[C_2\lambda^{-1}T(i,j)^{-1}]\}^{-1},\tag{2}$$

式中:$\varepsilon(i,j)$为空间点辐射率;u 为光电转换系数;C_1 为第一辐射常数;C_2 为第二辐射常数,$C_2=1.439\times10^{-2}$ m/K;$T(i,j)$为取像时刻图像点(i,j)处对应焊接区瞬时温度;R 在视觉系统安装后即可视为常值。

在足够短的时间内,将同一目标通过带宽 $\Delta\lambda$ 相同但中心波长分别为 λ_1、λ_2 的两波光片,成像于同一个摄像机上,得到两幅图像,设一个物理空间点的图像灰度(对应于辐射)在两幅图像的相同位置(i,j)上分别为 $Q_1(i,j)$、$Q_2(i,j)$,由式(2)及比色图像比色值的定义,其辐射信号之比值 $r(i,j)$为

$$r(i,j)=\frac{Q_1(i,j)}{Q_2(i,j)}=\frac{\lambda_2{}^5}{\lambda_1{}^5}\exp[C_2(\frac{1}{\lambda_2T(i,j)}-\frac{1}{\lambda_1T(i,j)})]。\tag{3}$$

将式(3)代入式(1),将分子分母相同常数项约去,得

$$i_e=\frac{\sum_{j=1}^{n}\sum_{i=1}^{m}\exp[\frac{C_2}{T(i,j)}(\frac{1}{\lambda_2}-\frac{1}{\lambda_1})]\cdot(i-i_c)}{\sum_{j=1}^{n}\sum_{i=1}^{m/2}\exp[\frac{C_2}{T(i,j)}(\frac{1}{\lambda_2}-\frac{1}{\lambda_1})]-\sum_{j=1}^{n}\sum_{i=(m/2+1)}^{m}\exp[\frac{C_2}{T(i,j)}(\frac{1}{\lambda_2}-\frac{1}{\lambda_1})]}。\tag{4}$$

视觉传感器摄入图像分为有焊缝区域与无焊缝区域,对存在焊缝的区域,设在 i 方向的焊缝区间为 $i\in[b_1,b_2]$,$j\in[1,n]$。由于焊缝没有金属表面,由气体组成,而气体在视觉系统选定波长区域内为选择性辐射体[3],CCD 感应到的信号强度很低。为方便讨论,设焊缝区域温度为恒定温度 T_c,其值近似于环境温度,即

$$T(i,j)=T_c,\ i\in[b_1,b_2];j\in[1,n]。\tag{5}$$

由于 T_c 很小,对试验选取比色系统两滤光片的中心波长分别为$\lambda_1=0.635\ \mu$m,$\lambda_2=0.680\ \mu$m。对应的函数 $\exp[C_2/T_c(1/\lambda_2-1/\lambda_1)]$ 值趋近于零,可将函数视为

$$\exp[\frac{C_2}{T_c}(\frac{1}{\lambda_2}-\frac{1}{\lambda_1})]=0,$$
$$i\in[b_1,b_2];\quad j\in[1,n]。\tag{6}$$

视觉场内无焊缝的区域,$\exp[C_2/T_c(1/\lambda_2-1/\lambda_1)]$ 是一个不为零且随温度而变化的数值。

又由焊缝中心与电弧中心的相对位置关系,焊接区域分为两种情况。

(1) 在电弧中心两侧对应点无焊缝存在时,焊接热流对称分布,从而焊接温度场在与焊接速度垂直的方向关于电弧中心也是对称的,即

$$T(i,j)=T(2i_c-i,j)。\tag{7}$$

从而有

$$\exp[\frac{C_2}{T(i,j)}(\frac{1}{\lambda_2}-\frac{1}{\lambda_1})]=\exp[(\frac{C_2}{T(2i_c-i,j)})(\frac{1}{\lambda_2}-\frac{1}{\lambda_1})],$$
$$i\notin[b_1,b_2];\quad j\in[1,n]。\tag{8}$$

此时,偏心公式分子、分母对称部分相互抵消为零。

(2) 在电弧中心两侧对称位置存在焊缝时,此时焊缝中心偏离电弧中心,函数值 $\exp[C_2/T_c(1/\lambda_2-1/\lambda_1)]$ 关于电弧中心左右不对称。将式(6)代入式(4),偏心公式分子、分母求和后余下与焊缝区域对称位置的函数值 $\exp[C_2/T_c(1/\lambda_2-1/\lambda_1)]$。

而焊接区域由(1)、(2)两种情况组成,因此,偏心公式可综合为

$$i_e=\frac{\sum_{j=1}^{n}\sum_{i=2i_c-b_2}^{2i_c-b_1}\exp[\frac{C_2}{T(i,j)}(\frac{1}{\lambda_2}-\frac{1}{\lambda_1})]\cdot(i-i_c)}{\sum_{j=1}^{n}\sum_{i=2i_c-b_2}^{2i_c-b_1}\exp[\frac{C_2}{T(i,j)}(\frac{1}{\lambda_2}-\frac{1}{\lambda_1})]}。\tag{9}$$

式(9)即为焊接比色图像偏心与焊缝中心与电弧中心的偏差值、焊接区各点离散温度值间的简化关系模型。$(i-i_c)$是焊缝中心与电弧中心的偏差,模型输出比色图像偏心值 i_e。值得说明的是,当焊缝中心与电弧中心完全对准时,偏心公式的分子、分母将全部抵消为零,此时,计算机程序计算值也为

零，即当焊缝中心与电弧中心偏差值为零时，由比色图像偏心算法计算出的偏心值也为零，这与实际情况相符。

从式(9)可看出，模型计算简便，对每幅比色图像标定出电弧中心、图像分割后即可进行比色值偏心 i_e 的计算。

3　关系模型的数值化及特性

为对式(9)有数值上的理解，对关系模型数值化，首先建立某一试验条件下焊接瞬态温度场。

3.1　TIG 焊接温度场模型及数值模拟

根据 Fourier 传热定律和能量守恒定律，对有限厚薄板，可建立平面传热问题的控制方程[4]，即焊件的瞬态温度场 $T(x, y, t)$ 应满足以下方程

$$c\rho\frac{\partial T}{\partial t}=\kappa\left(\frac{\partial^2 T}{\partial x^2}+\frac{\partial^2 T}{\partial y^2}\right)+Q, \tag{10}$$

式中：T 为工件表面瞬时温度；ρ 为材料密度；c 为比热容；κ 为导热系数；Q 为内部热源。

3.1.1　热源模型

仿真试验采用 TIG 焊接，其热源分布一般采用高斯移动热源模型，即

$$q=q^*_{max}\exp(-br^2), \tag{11}$$

式中：q 为电弧有效半径处的表面热流；q^*_{max} 为加热斑点中心的最大比热流，与焊接工艺参数有关；b 为热源集中系数；r 为距热源中心的距离。

3.1.2　边界条件

焊接边界与周围介质进行换热，热量的散失主要有热辐射换热和对流换热。根据实际焊接情况，采用第二、三类综合的边界条件，对于某一与流动的气体或液体接触的固体表面微元，其对流换热通过对流、辐射换热综合系数 α_s 与固体表面温度 T 和周围环境温度 T_∞ 之差成比例[4] 为

$$\kappa=\frac{\partial T}{\partial n}=\alpha_s(T-T_\infty), \tag{13}$$

式中：n 边界表面外法线方向。

3.1.3　初始条件

在 $t=t(0)$ 时刻，温度等于初始温度值，即

$$T=T(0)。 \tag{14}$$

温度场数值模拟的基本假设是，忽略 z 向温度变化，温度场数值模拟作二维传热问题处理；金属熔体与固体热物性取常数，并取为热物理性质各个方向相同。常数值见文献[5]。

3.1.4　焊接仿真试验条件

焊接温度场数值模拟采用的工艺试验条件见表 1。

表 1　焊接仿真试验条件

Table 1　Welding experimental conditions

焊接方法	Q235 mm× mm× mm	保护气流量 q/(L·min^{-1})	电流 I/A	电压 U/V	焊接速度 v/(m·min^{-1})
TIG	200×150×4	10	80	18	0.36

以上条件下，式(10)~式(14)协调有解，可得到焊接温度场基本数据见图 1。比色视觉系统分辨率为 0.06 mm/pixel。

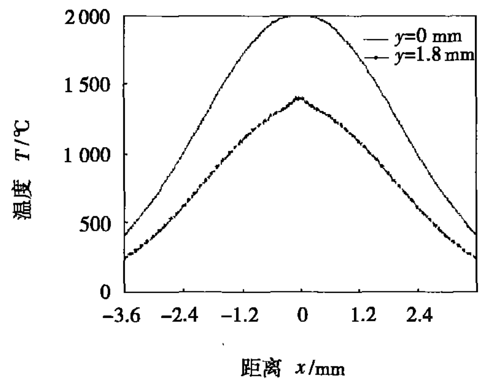

图 1　数值模拟的焊接温度场

Fig. 1　Simulated welding temperature field

从图 1 中可看出熔宽在 3.5 mm 左右，与实测熔池宽度相当，温度场数值模拟基本符合实际工艺参数条件下的熔池数据。根据比色图像与偏心公式，并由模拟得到的焊接温度场离散数据，可计算图像各点的 $\exp=[C_2/T(i,j)(1/\lambda_2-1/\lambda_1)]$ 值，取视觉图像大小分别为 m 方向 120 个像素，n 方向 40 个像素，从而 i 方向至图像中心为 60.5。$\exp[C_2/T(i,j)(1/\lambda_2-1/\lambda_1)]$ 函数值形貌在无焊缝时分布如图 2 所示。

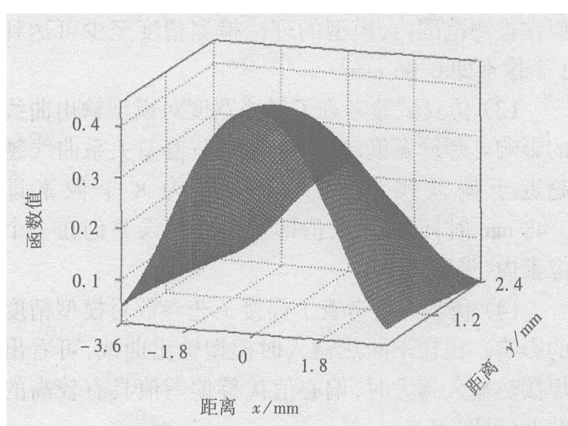

图 2　焊接区各点 $\exp[C_2/T(i,j)(1/\lambda_2-1/\lambda_1)]$ 值形貌

Fig. 2　3-distribution of function value

3.2 模型的数值解及特性

由焊接区各点的 $\exp[C_2/T(i,j)(1/\lambda_2-1/\lambda_1)]$ 分布,根据式(9)可计算出不同 $(i-i_c)$ 对应的图像偏心值 i_e,表 2 列出了在单侧 0~36 像素范围内的 i_e 和 $(i-i_c)$ 部分数值解,图 3 为[0,36] 范围内模型输入与输出关系曲线。

表 2 模型部分数值解(I=160 A)(单位:像素)

Table 2 Partial numerical solution of model(when I=160 A)(unit: pixel)

序号 / 项目	1	2	3	4	5	6	7	8	9	10
偏差值 $(i-i_c)$	0	4	8	12	16	20	24	28	32	36
偏心值 i_e	0	4.001 0	8.001 7	12.002 5	16.003 3	20.004 1	24.005 0	28.005 9	32.006 9	36.007 9

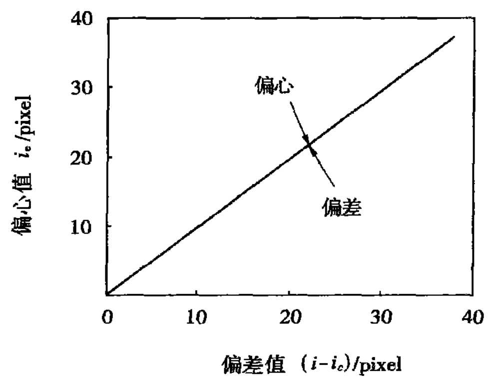

图 3 偏心值 i_e 与偏差值 $(i-i_c)$ 线性关系

Fig. 3 Relation curve between offset distance and offset value

从表 2 及图 3 可以看到:(1) 输出量 i_e 与输入量 $(i-i_c)$ 有较好的比例为 1 的线性关系。这就证明了以焊接比色图像中检测到的偏心值来代替焊缝中心偏离电弧中心的偏移量即焊缝偏差值的理论可行性。

(2) 输入实际的中心偏差值 $(i-i_c)$,输出量 i_e 与 $(i-i_c)$ 的差值最大不到一个像素,最大误差在最侧端点即第 36 个像素处。模型虽向两端误差发散,但在检测范围内,模型的理论检测精度至少可达到 1 个像素即 0.06 mm。

(3) 仿真试验考查了焊缝宽度对模型输出曲线的影响。焊缝宽度越小,则偏心与偏差关系曲线越趋近于偏差线,而在焊缝宽度为 8 个像素即 0.48 mm 时,误差最大值即端点处的误差仍在 1 个像素内(见图 4a)。

(4) 仿真试验考查了焊接工艺参数对模型精度的影响。比较不同热输入时模型输出曲线,可看出焊接热输入越大时,偏心值代替偏差值具有较高的精度(见图 4b)。

3.3 模型误差分析

以比色图像偏心值代替焊缝中心与电弧中心的偏差的仿真证明过程中,温度场的模拟采用数值模拟方法来证明模型的准确性,其中各项系数取常数,而导热系数 κ、低碳钢的密度 ρ、表面对流换热系数 α_s、材料的比热容 c 等都随温度有些变化,会导致温度场的模拟与实际温度场有偏差,从而影响到模型精度的验证。但从理论上分析,以变热物性参数代

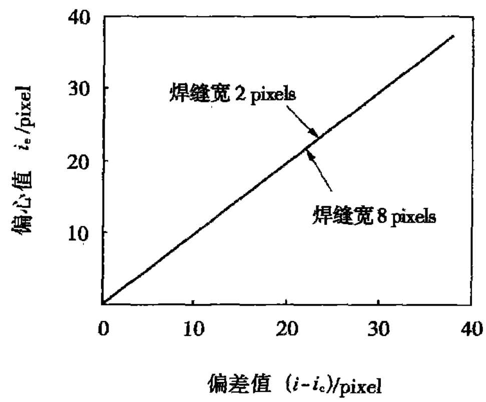

(a) 焊缝宽度的影响

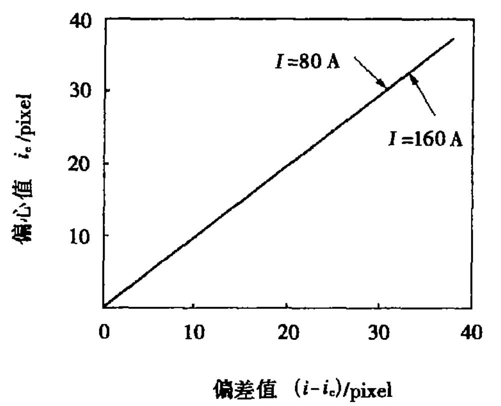

(b) 焊接电流的影响

图 4 焊缝宽度和焊接工艺参数对模型关系曲线的影响

Fig. 4 Influence of welding parameters on model

[下转第 20 页]

环后,残留在物体中的引起物体应力和变形的应变,它是物体产生应力和变形的根源,主要由热循环中的最高加热温度和结构的拘束条件来决定。

(2)如果不追究变形的过程,可以用固有应变为中间变量,通过一次弹性板单元有限元分析求解整个复杂结构的变形。

(3)通过典型结构的焊接变形的预测和船板的热应力弯曲成形变形计算的实例,验证了固有应变为基础的弹性板单元有限元残余变形预测法在热加工过程中应用的可能性。

参考文献:

[1] Ueda Y, Yuan M G. A predicting method of welding residual stress using source of residual (report III)[J]. Trans of Joining and Welding Research Institute, 1993, 22(1): 157—168.

[2] Luo Y, Murakawa H, Ueda Y. Prediction of welding deformation and residual stress by elastic FEM based on inherent strain (report I)[J]. Trans of Joining and Welding Research Institute, 1997, 26(2): 49—57.

[3] Ueda Y, Yamakawa T. "Analysis of thermal elastic-plastic stress and strain during welding", IIW Doc. X—616—71(1971), also trans [J]. Japan Welding Soc., 1971, 2(2): 90—100.

[4] 纪卓尚, 刘玉君, 孙振烈, 等. 船体曲面钢板水火加工成型工艺的理论与应用研究[J]. 中国造船, 1998(10): 117—123.

[5] Yukio Ueda, Hidekazu Murakawa, Ahmed Mohamed Rashwan, *et al*. Development of computer aided process planning system for plate bending by line-heating (report 1)-relation between the final form of plate and the inherent strain[J]. Trans of Joining and Welding Research Institute, 1991, 20(2): 129—139.

作者简介:罗 宇,男,1961年出生,工学博士,教授。主要研究方向为焊接力学,发表论文40余篇。

Email: luoyu@sjtu.edu.cn

[上接第16页]

替常热物性参数得到的温度场数据会有差异,但对偏心值与偏差值关系曲线不会产生影响。

4 结 论

(1)提出了焊接比色图像偏心的概念,并给出焊接比色图像偏心的计算公式。

(2)采用小范围内窄带滤光技术,推导并建立了焊接比色图像偏心与焊接区各点温度及焊缝中心与电弧中心偏差的数值关系模型。

(3)从理论上证明了模型的输出与输入有良好的线性关系及以比色图像偏心代替焊缝中心偏离电弧中心值的可行性,且模型对焊缝宽度及焊接工艺参数的变化具有良好的鲁棒性。

参考文献:

[1] 潘际銮. 现代弧焊控制[M]. 北京: 机械工业出版社, 2000. 301—361.

[2] 高向东, 罗锡柱. 基于卡尔曼滤波的焊缝检测技术研究[J]. 机械工程学报, 2004, 40(4): 172—176.

[3] 陈永甫. 红外辐射器件与典型应用[M]. 北京: 电子工业出版社, 2006. 1—30.

[4] 雷卡林 H H. 焊接热过程计算[M]. 北京: 机械工业出版社, 1980. 21—121.

[5] 赵镇南. 传热学[M]. 北京: 高等教育出版社, 2002. 344—367.

作者简介:高向东,男,1963年8月出生,工学博士,教授。主要从事机器视觉和自动控制等研究工作,主持完成国家自然科学基金和广东省自然科学基金等课题多项,发表论文50余篇。

Email: gaoxd666@126.com

MAIN TOPICS, ABSTRACTS & KEY WORDS

Numerical simulation of molten pool temperature field for TIG welding of pure copper without preheating LEI Yu-cheng, YU Wen-xia, LI Cai-hui, CHENG Xiao-nong (School of Materials Science and Engineering, Jiangsu University, Zhenjiang 212013, Jiangsu, China). p1—4

Abstract: Welding process is a rapid and quite non-uniform physicochemical metallurgy process, and molten pool is always one of the important areas for welding simulation. According to the principle of conservation of energy and characteristics of tungsten inert gas (TIG) welding, the numerical model of non-steady TIG welding pool shape under moving arc was established. The heat enthalpy conception and the heat model of surfaced bielliptic distribution were introduced and the demands of welding numerical simulation was primely satisfied. The TIG welding of thick-wall pure copper adopting Ar+ N_2 without preheating was studied. The comparison between the experiment value and the calculation with different process parameters showed that the model and practical course match well, and the reliability and correctness of the model are proved.

Key words: without preheating; pure copper; argon tungsten-arc welding; temperature field; numerical simulation

Microstructures of W-17% Co coating produced by plasma melt spraying (I) GUO Mian-huan, LIU Ai-guo, ZHAO Min-hai, QU Jun-zhang (State Key Laboratory of Advanced Welding Production Technology, Harbin Institute of Technology, Harbin 150001, China). p5—8

Abstract: W-17% Co metallic ceramic coating was prepared by plasma melt spraying (PMS) on low carbon steel Q235. Metallurgical bonded coating with high bonding strength had been obtained, and the key problem of low bonding strength for ceramic coating had been solved. Microstructures were analyzed with optical microscope, SEM, TEM and EDS. The results showed that a joint produced by PMS process was similar to a welded joint, and consisted of coating, fusion zone, diffusion zone, and heat affected zone. Microstructures of PMS coating are very different from the sprayed ones. Phases in the coating are very complicated and consisted mainly of M_6C (Fe_3W_3C or Co_3W_3C), WC, γ-Fe, Co_3O_4, γ-Co, FeW_3C, Fe_2W and W_2C. These phases distribute in different regions in the coating. According to the microstructures, the coating can be divided into surface layer, metallurgical reaction layer and bottom layer.

Key words: plasma melt spraying; W-17% Co coating; microstructures of coating

CO_2 laser beam welding of aluminum alloy with additional current via filler wire XIAO Rong-shi[1], ZUO Tie-chuan[1], Ambrosy G[2], Hügel H[2] (1. National Center of Laser Technology, Beijing University of Technology, Beijing 100022, China; 2. Institut für Strahlwerkzeuge (IFSW), University of Stuttgart, Stullart D—70569, Germany). p9—12

Abstract: By making use of the magnetohydrodynamic effect of electrical current, a new aspect of CO_2 laser beam welding of aluminum alloy with an electrical current addition was reported. During the laser beam welding, an electrical current was supplied to the weld pool via the filler wire. By connecting one pole of a DC power source with the filler wire and the other with the workpiece in the rear of the weld pool, a closed electric circuit was built. It is found that this new technique increases the welding efficiency and flexibility, and improves the process stability—the weld depth and area increase considerably and the bead ripples become finer and more uniform with the increase of the current. Further experimental results demonstrate that the resistive heating of the wire has less influence. Thus it can be concluded that the influence of the current on CO_2 laser beam welding of aluminum alloy results from the electromagnetic effect of current.

Key words: CO_2 laser beam welding; aluminum alloy; electrical current; welding efficiency; processing stability

A new approach to detect weld seam based on offset-distance arithmetic of welding colorimetry image GAO Xiang-dong, CHEN Zhang-lan, CHEN Yong-ping (Faculty of Mechanical and Electrical Engineering, Guangdong University of Technology, Guangzhou 510090, China). p13—16, 20

Abstract: A new method to detect the weld seam centerline by calculating the offset-distance based on welding colorimetry image was proposed. The concept of offset-distance was defined and the offset-distance arithmetic that analyzes the welding colorimetry image was applied to obtain the deviation between the weld seam centerline and the arc column center. Based on the offset-distance formula, the relationship of some factors such as the signal intensity of CCD, welding temperature field, center wavelength of a narrow-band filter, emissivity of welding region, weld seam and the radiant intensity was obtained. Model giving the relation between the offset-distance of welding colorimetry image and the discrete numerical welding temperature field and the deviation between the weld seam centerline and the arc column center had been established. The numerical solution of the model had been presented and the relation curve had been shown. The conclusion indicates that the output parameter of the model which is the offset-distance of the welding colorimetry image and the input parameter which is the weld seam centerline has a good linear relation. Therefore the deviation between the weld seam centerline and the weld arc column center which is hardly detected directly from the welding visual image can be calculated by the offset-distance which is easily obtained from the welding colorimetry image. The factors influenced the accuracy of the model have been analyzed. The model makes the application of the offset-distance of welding colorimetry image for detecting the actual weld seam centerline more practical and simpler.

Key words: weld colorimetry image; offset-distance; weld seam deviation; model

A method to predict residual distortion based on inherent strain and its application to heating processes LUO Yu[1], DENG De-an[2], JIANG Xiao-ling[1], ZHU Zhi-feng[1] (1. The School of Naval Architecture, Ocean and Civil Engineering, Shanghai Jiaotong University, Shanghai 200030, China; 2. College of Mechanical Engineering, Chongqing University, Chongqing 400044, China). p17—20

Abstract: A method to predict residual deformation based on inherent strain was introduced. The proposed method was applied to predict welding deformation for the tank with lower temperature and plate bending deformation by line heating. Feasibility of the proposed method was also verified.

Key words: inherent strain; welding deformation; plate bending; finite element method

SVM classifier for wire extension monitoring using arc sound signal in GMAW MA Yue-zhou, QU Min, CHEN Jian-hong (Key Laboratory of Non-ferrous Metal Alloys, the Ministry of Education, Lanzhou university of Technology, Lanzhou 730050, China). p21—26

Abstract: To find the approach of monitoring welding quality by arc sound, the frequency spectral characteristics of the arc sound signals in short circuit GMAW process were analyzed. The concept of tone channel of welding arc was introduced, which was considered a time dependent distributed parameters system influenced by welding parameters, arc behavior and the other factors. The LPC (linear prediction coding) model of the arc sound signal was an estimation of transmission properties of the tone channel. The spectrum analyses indicated that the frequency characteristics of the arc sound signal were closely related to the wire extension, but the correlation presented high complexity and nonlinearity. The classifiers based on SVM (support vector machine) for monitoring wire extensions were established, in which the input vectors of sample sets were built with the predictor coefficients and reflection coefficients of LPC model of the arc sound signals. The training and testing results showed that the SVM classifiers with different kernels are all capable of classifying the wire extension, whose performances were obviously better than that of the RBF (radial basis function) neural networks under the same condition, and present good capability of generalization at small sample set. The classifiers with 3rd order polynomial kernel trained with reflection coefficients input vectors has the best accuracy, i.e. over 98%. The study indicated that forming characteristic vectors by the LPC coefficients of arc sound to build SVM pattern recognition model is a feasible way for welding parameters monitoring.

Key words: welding arc sound; linear prediction coding model; support vector machine application; gas metal arc welding; welding parameter monitoring

Solution and application of energy distribution models based on point heat sources during gas metal arc welding process WANG Hou-xiao[1,2], SUN Jun-sheng[1], WEI Yan-hong[2], ZHENG Yuan-yuan[1] (1. School of Materials Science and Engineering, Shandong University, Jinan 250061, China; 2. State Key Laboratory of Advanced Welding Production Technology, Harbin Institute of Technology, Harbin 150001, China). p27—30

Abstract: Calculations were made for the transient solution of welding thermal process with a point heat source moving on the workpiece with three different energy distribution models based on point heat sources for gas metal arc welding (GMAW) process. These three distribution models of energy input for GMAW process were evaluated by the comparison between the predicted weld junction and the measured results. Moreover, weld junction of the weldments from low carbon steel Q195 and low alloy steel JG590 via GMAW technique were predicted using the developed string heat source model. Experiments for both Q195 steel and JG590 steel were conducted. The predicted weld cross sections had a good agreement with the experimental measurements. Current equations for $t_{8/5}$ calculation were evaluated. Based on the calculated results from GMAW thermal process, microstructure and hardness of JG590 steel fusion zone were successfully predicted with the continuous cooling transformation diagram.

Key words: gas metal arc welding; point heat sources; energy distribution models; prediction of microstructure and hardness

Safe assessment for overmatching welded joint of offshore pipeline LIU Ming-liang, ZHANG Yu-feng, HUO Li-xing, DENG Cai-yan (School of Materials Science and Engineering, Tianjin University, Tianjin 300072, China). p31—34

Abstract: For given crack size and load, structure integrity assessment procedure (SINTAP) sponsored by the European Commission was applied to assess the overmatching welded joints of the API 5L X65 pipeline steel with surface flaw at the weld toe. The assessment was carried out according to limit load solutions and the CTOD (crack tip opening displacement) test result. The failure line of level 2 of the weld was derived from the tensile test results. The result of the assessment showed that the point (L_r, K_r) is located within the failure line of analysis level 2. So the overmatching welded joint of the pipeline is safe. This study laid the foundation of application of SINTAP to pipeline structure assessment.

Key words: structure integrity assessment procedure; overmatching; failure assessment diagram